Electronic Supplementary Information: Three-dimensional atomic models from a single Z-contrast image: verification by electron tomography and opportunities

A. De Backer,[a] L. Jones,[b] I. Lobato,[a] T. Altantzis,[a] B. Goris,[a] P.D. Nellist,[b] S. Bals,[*a] and S. Van Aert[*a]

[a] *Electron Microscopy for Materials Research (EMAT), University of Antwerp, Groenenborgerlaan 171, B-2020 Antwerp, Belgium*
[b] *Department of Materials, University of Oxford, OX13PH Oxford, United Kingdom*
[*] *Corresponding authors: sandra.vanaert@uantwerpen.be, sara.bals@uantwerpen.be*

S1 Drift correction

Prior to the statistics-based atom-counting method, the influence of sample drift during the acquisition of the experimental images can be post-compensated by using the known lattice proportions and angles between two planes at each specimen orientation. For example, for FCC gold in [001] orientation, the lattice proportion between the projected a- and b-direction equals 1 and the angle equals 90°. The procedure for drift compensation starts by finding all the atomic column positions from which the average lattice parameters and the angles between two planes are calculated. Then, the affine transformation T, which includes horizontal shear (α) and vertical scaling (β)

$$T\begin{bmatrix}x\\y\end{bmatrix}=\begin{bmatrix}1&\alpha\\0&\beta\end{bmatrix}\begin{bmatrix}x\\y\end{bmatrix},$$

is obtained by minimizing the following cost function:

$$\chi^2=\left(1-\frac{r_{\text{th}}}{r_{\text{exp}}(\alpha,\beta)}\right)^2+\left(1-\frac{\theta_{\text{th}}}{\theta_{\text{exp}}(\alpha,\beta)}\right)^2$$

where r_{th} and r_{exp} are the theoretical and experimental lattice proportion, and θ_{th} and θ_{exp} are the theoretical and experimental angles between the two planes, respectively. The images are then drift compensated by applying this affine transform.

S2 Details of statistical atom-counting analysis Au nanorod

Using statistical parameter estimation theory, the scattering cross-sections can be quantified atomic column-by-atomic column by fitting an empirical imaging model to the experimental, drift corrected, images[1–5]. This empirical imaging model consists of a sum of Gaussian peaks describing the atomic column intensities:

$$f_{kl}(\theta)=\zeta+\sum_{n=1}^{N}\eta_n\exp\left(\frac{-(x_k-\beta_{x_n})^2-(y_l-\beta_{y_n})^2}{2\rho^2}\right) \quad (1)$$

where $\theta=(\beta_{x_1},\ldots,\beta_{x_N},\beta_{y_1},\ldots,\beta_{y_N},\rho,\eta_1,\ldots,\eta_N,\zeta)^T$ are the unknown structure parameters with ρ being the width of the Gaussian peak, η_n the height of the nth Gaussian peak, β_{x_n} and β_{y_n} the x- and y-coordinate of the nth atomic column, respectively, and N the total number of analyzed atomic columns. The unknown parameters θ of the model are estimated in the least squares sense. The estimated scattering cross-sections $V_n=2\pi\eta_n\rho^2$ then correspond to the volumes under the estimated Gaussian peaks. The fitted models for the drift corrected images of Figs. S1-S3(a) are shown in Figs. S1-S3(b). The models are in excellent agreement with the experimental data demonstrating their good quality. Next, the estimated scattering cross-sections can be visualized in a histogram as illustrated in Figs. S1-S3(c). Ideally, this histogram would consist of isolated components. However, due to a combination of instabilities of the microscope and sample, and noise effects, the components are smeared out. Therefore, the estimated scattering cross-sections are regarded as a statistical draw from an unknown probability distribution consisting of a superposition of Gaussian components, the

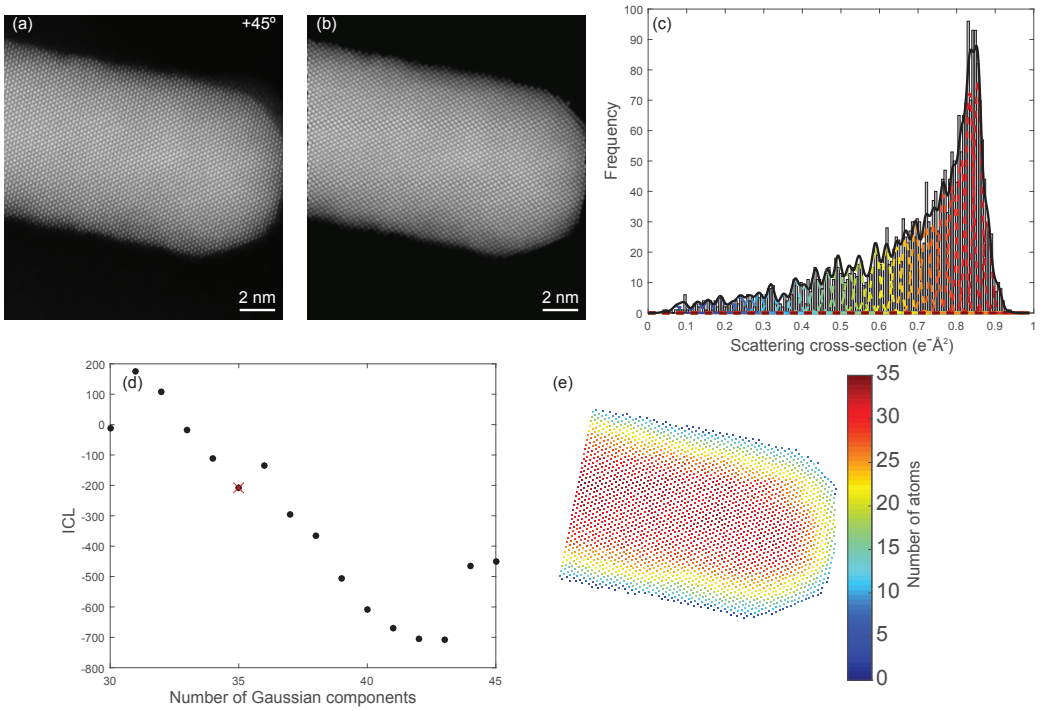

Fig. S1 Statistical atom-counting procedure for a Au nanorod along $[110]$ **direction (**$+45°$**)** (a) Experimental drift corrected atomic resolution ADF STEM projection image, (b) Refined model, (c) Histogram of scattering cross-sections of the Au columns. The black curve shows the estimated mixture model; the individual components are shown as colored curves which correspond to the colors for the number of atoms in (e), (d) ICL criterion evaluated as a function of the number of Gaussian components in a mixture model, the selected minimum is indicated by a red cross, and (e) Number of atoms per column.

so-called Gaussian mixture model:

$$f_{\text{mix}}(V_n;\Psi_G) = \sum_{g=1}^{G} \pi_g \frac{1}{\sqrt{2\pi}\sigma} \exp\left(\frac{-(V_n-\mu_g)^2}{2\sigma^2}\right). \tag{2}$$

This model defines the probability that a specific scattering cross-section value V_n would be estimated for a particular atomic column n. The vector $\Psi_G = (\pi_1,\ldots,\pi_{G-1},\mu_1,\ldots,\mu_G,\sigma)^T$ contains the unknown parameters π_g, μ_g, and σ being the mixing proportion of the gth component, the mean scattering cross-section of the gth component, and the width of the components, respectively. The parameters Ψ_G can be estimated from the experimental scattering cross-sections using the maximum likelihood estimator for a given number of components G[2,6–8]. In practice, the value of G is unknown and has to be inferred from the available scattering cross-sections as well. The number of significant components, i.e. the model order G can be retrieved by evaluating the so-called integrated classification likelihood (ICL) criterion, which is shown in Figs. S1-S3(d). This order selection criterion balances the model fit against the model quality. Indeed the model fit will typically improve for increasing number of components and more details in the available set of scattering cross-sections will be described. However, for high-order models, these details are random and as a consequence the model quality will degrade with the model order. The estimated model order is given by the number of components for which ICL reaches a minimum, which is indicated by a red cross in Figs. S1-S3(d). In practice this minimum often corresponds to a local optimum rather than a global optimum[2]. Figs. S1-S3(c) shows the estimated Gaussian mixture model. Based on this estimated probability distribution, the number of atoms can be identified by assigning each scattering cross-section to the component of the mixture model with the largest probability to generate this scattering cross-section. The atom-counts for every column of the nanorod are shown in Figs. S1-S3(e).

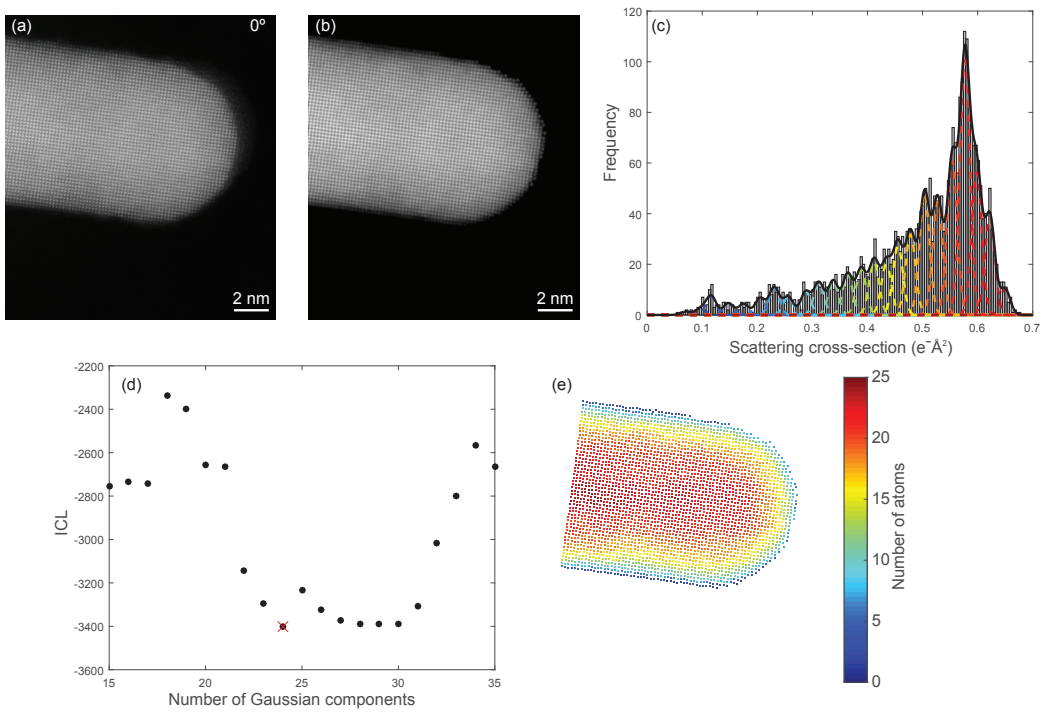

Fig. S2 Statistical atom-counting procedure for a Au nanorod in $[100]$ orientation ($0°$) (a) Experimental drift corrected atomic resolution ADF STEM projection image, (b) Refined model, (c) Histogram of scattering cross-sections of the Au columns. The black curve shows the estimated mixture model; the individual components are shown as colored curves which correspond to the colors for the number of atoms in (e), (d) ICL criterion evaluated as a function of the number of Gaussian components in a mixture model, the selected minimum is indicated by a red cross, and (e) Number of atoms per column.

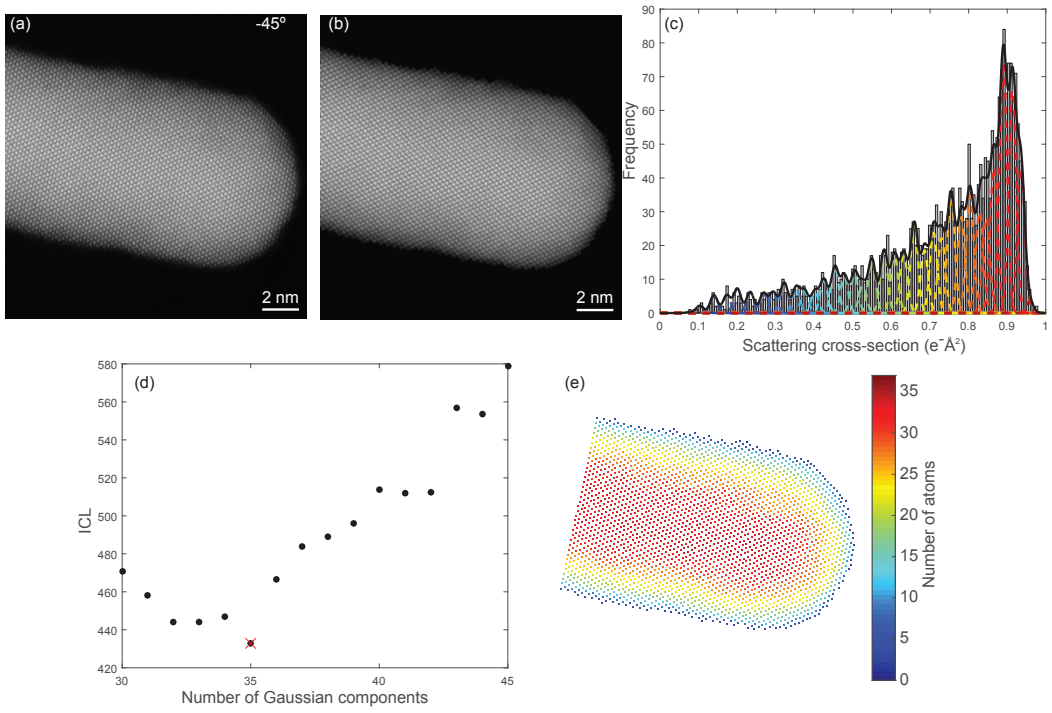

Fig. S3 Statistical atom-counting procedure for a Au nanorod in $[110]$ orientation ($-45°$) (a) Experimental drift corrected atomic resolution ADF STEM projection image, (b) Refined model, (c) Histogram of scattering cross-sections of the Au columns. The black curve shows the estimated mixture model; the individual components are shown as colored curves which correspond to the colors for the number of atoms in (e), (d) ICL criterion evaluated as a function of the number of Gaussian components in a mixture model, the selected minimum is indicated by a red cross, and (e) Number of atoms per column.

S3 Statistical atom-counting analysis for the heating experiment

For the heating experiment, atomic resolution images have been taken of the right part of the nanodumbbell and nanorod, before and after heating, respectively. These experimental images are shown in Figs. S4-S5(a). Since a very large number of atomic columns is present in these atomic resolution images a slightly adapted procedure as compared to the atom-counting of the previous Au rod has been applied. It has been illustrated by De Backer et al. that the number of atomic columns per component N/G in the Gaussian mixture model should be large enough[2]. However, when N/G is too large for some components (corresponding to e.g. a high thickness) with respect to other components (with e.g. a small thickness), the number of components in the Gaussian mixture model will be overestimated. For the acquired images, there is such a disproportion for N/G for different thicknesses of the atomic columns: there are too many columns with a similar thickness in the thicker part of the nanoparticle. In order to circumvent this problem, the number of atomic columns that is used in the statistical atom-counting analysis is limited so that an optimal N/G value is obtained. These analyzes are shown in Figs. S4-S5. The (b) panels of these figures show the refined models of the experimental images, the (c) panels show the histograms of the scattering cross-sections of the Au columns with overlying the estimated mixture model and its individual components in color, the (d) panels show the ICL criterion evaluated as a function of the number of Gaussian components in the mixture model, and the (e) panels shown the number of atoms per column for the analyzed atomic columns. The locations of the components of the estimated Gaussian mixture models, which can be read out from the x-axis of the (d) panels, are plotted as a function of the corresponding number of atoms in Fig. S6. This figure shows mutual agreement between the analyzes before and after heating. These locations are used to extrapolate the atom-counting results to all the atomic columns of the of the atomic resolution images. The averaged locations of the 2 curves of Fig. S6 are used as a library for fitting the Gaussian mixture model with fixed locations for the scattering cross-sections of all the atomic columns present in the atomic resolution images. An overview of the final Gaussian mixture models for all the atomic columns of each atomic resolution image are shown in Fig. S7.

S4 Procedure to generate initial 3D models for the nanodumbbell and nanorod

In order to obtain a reliable molecular dynamics (MD) relaxation, 3D atomic models are needed of the whole nanodumbbell and nanorod. The procedure to generate the initial 3D models of the whole nanodumbbell and nanorod starts by finding the affine transformation, which includes scaling, rotation, and translation, of the atomic resolution STEM images of the right part of the nanorod with respect to the low resolution images of Fig. 3. Then these affine transformations have been applied to the atomic column positions obtained from the high resolution STEM images. An extra alignment and rotation over the atomic columns has been performed in order to be able to use the same grid for the whole nanorod. For the remaining left part of the nanodumbbell and nanorod, the atomic columns positions and corresponding number of atoms are unknown and need to be estimated. The atomic column positions, on the one hand, could be retrieved by thresholding the image and using a two-dimensional aligned grid. The number of atoms of this part, on the other hand, has been calculated by using the atom-counting results of the right parts of the nanodumbbell and nanorod. From these known parts, the intensity as a function of the number of atoms is known and fitted by a second order polynomial. This relation has been used to approximate the number of atoms of the remaining part of the nanodumbbell and nanorod. In this manner, the overall shape of these parts has been estimated from the low resolution image and can be used for the MD simulations.

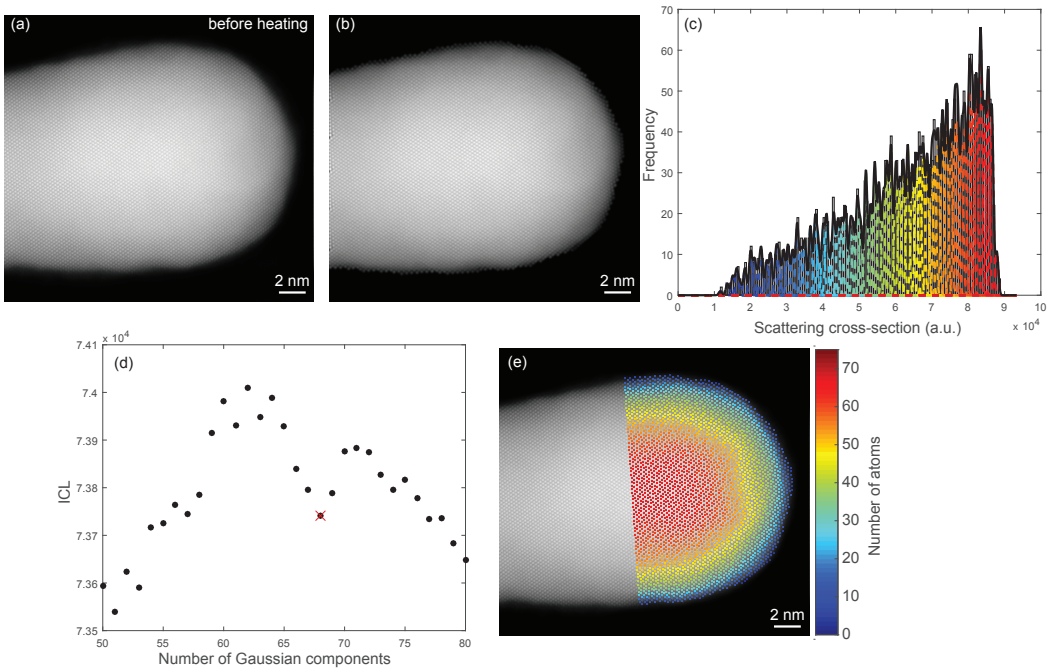

Fig. S4 Statistical atom-counting procedure for the Au nanodumbbell before heating (a) SmartAlign distortion corrected average of the experimental atomic resolution projection images along $[110]$ direction, (b) Refined model, (c) Histogram of scattering cross-sections of the Au columns. The black curve shows the estimated mixture model; the individual components are shown as colored curves which correspond to the colors for the number of atoms in (e), (c) ICL criterion evaluated as a function of the number of Gaussian components in a mixture model, the selected minimum is indicated by a red cross, and (e) Number of atoms per column.

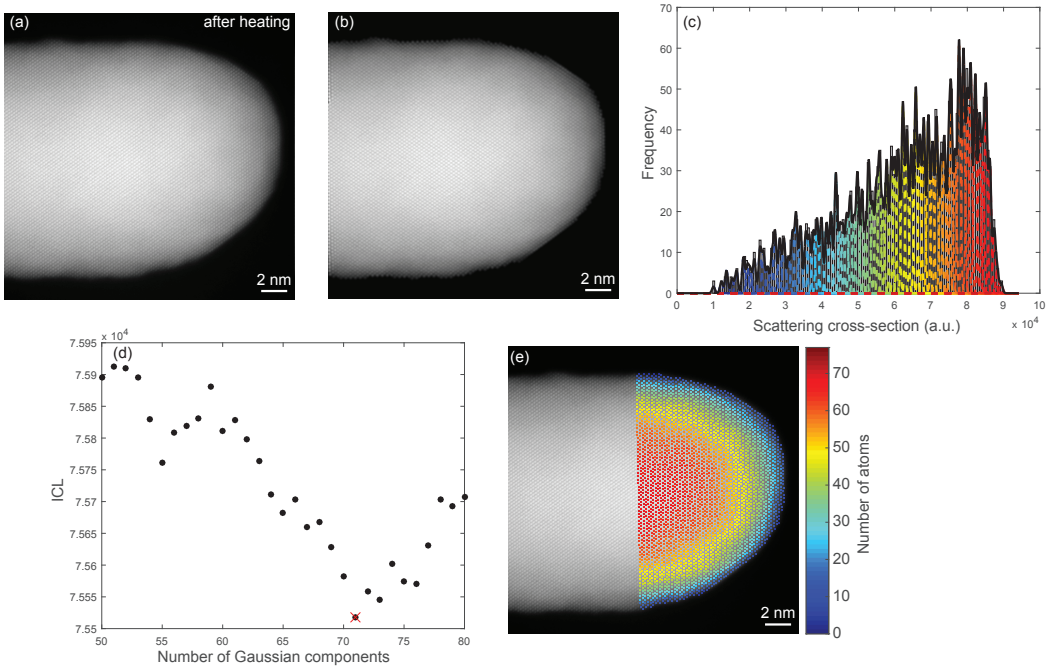

Fig. S5 Statistical atom-counting procedure for the Au nanorod after heating (a) SmartAlign distortion corrected average of the experimental atomic resolution projection images along $[110]$ direction, (b) Refined model, (c) Histogram of scattering cross-sections of the Au columns. The black curve shows the estimated mixture model; the individual components are shown as colored curves which correspond to the colors for the number of atoms in (e), (c) ICL criterion evaluated as a function of the number of Gaussian components in a mixture model, the selected minimum is indicated by a red cross, and (e) Number of atoms per column.

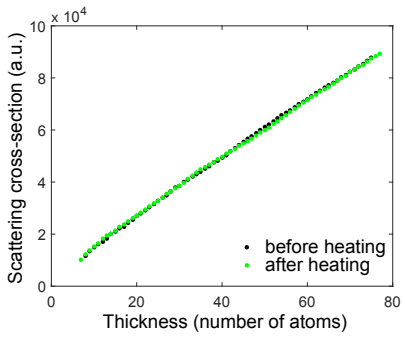

Fig. S6 Scattering cross-sections as a function of the thickness for the nanodumbbell and nanorod, before and after heating respectively.

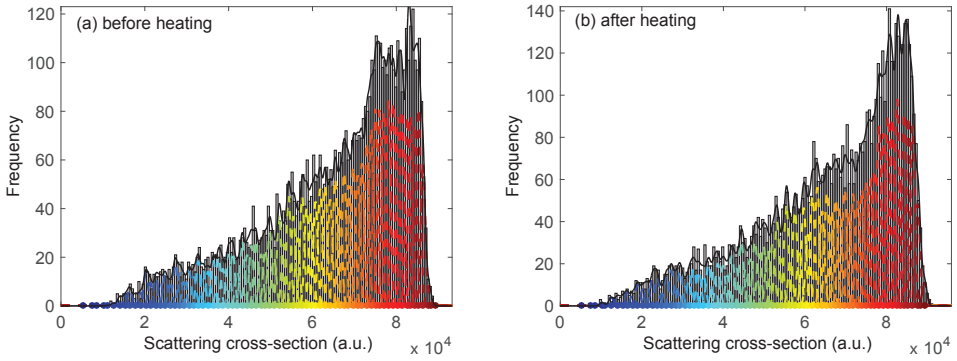

Fig. S7 Gaussian mixture models describing the distribution of the scattering cross-sections corresponding to all the projected atomic columns in the atomic resolution projection images for the nanodumbbell and nanorod, before and after heating, respectively.

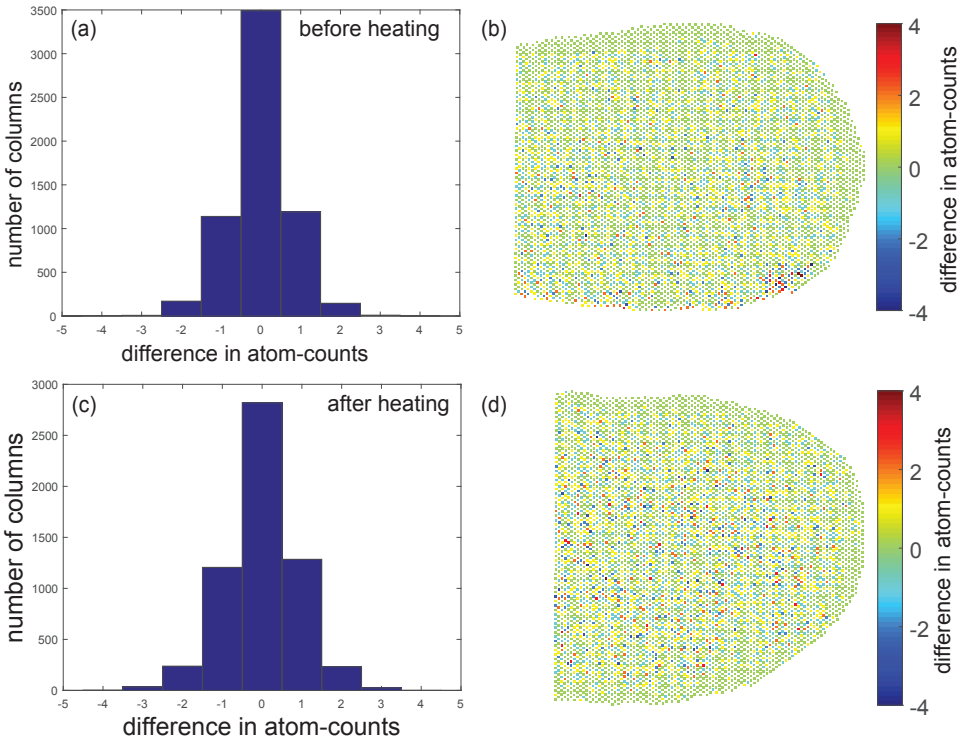

Fig. S8 Difference in atom-counts before and after relaxation per atomic column for the nanodumbbell and nanorod, before and after heating, respectively. The differences are presented in a histogram and an atomic column map. The differences are randomly distributed on the particle and are within the counting error.

References

1 S. Van Aert, J. Verbeeck, R. Erni, S. Bals, M. Luysberg, D. Van Dyck and G. Van Tendeloo, *Ultramicroscopy*, 2009, **109**, 1236–1244.

2 A. De Backer, G. T. Martinez, A. Rosenauer and S. Van Aert, *Ultramicroscopy*, 2013, **134**, 23–33.

3 A. J. den Dekker, J. Gonnissen, A. De Backer, J. Sijbers and S. Van Aert, *Ultramicroscopy*, 2013, **134**, 34–43.

4 S. Van Aert, A. De Backer, G. T. Martinez, A. J. den Dekker, D. Van Dyck, S. Bals and G. Van Tendeloo, *IUCrJ*, 2016, **3**, 71–83.

5 A. De Backer, K. H. W. van den Bos, W. Van den Broek, J. Sijbers and S. Van Aert, *Ultramicroscopy*, 2016, **171**, 104–116.

6 S. Van Aert, K. J. Batenburg, M. D. Rossell, R. Erni and G. Van Tendeloo, *Nature*, 2011, **470**, 374–377.

7 S. Van Aert, A. De Backer, G. T. Martinez, B. Goris, S. Bals and G. Van Tendeloo, *Physical Review B*, 2013, **87**, 064107.

8 G. McLachlan and D. Peel, *Finite Mixture Models*, John Wiley and Sons, inc., 2000.